

See discussions, stats, and author profiles for this publication at: <https://www.researchgate.net/publication/319396515>

Highly Sensitive Surface-Enhanced Raman Scattering (SERS)- Based Multi Gas Sensor : Au Nanoparticles Decorated on Partially Embedded 2D Colloidal Crystals into Elastomer

Article in *ChemistrySelect* · August 2017

DOI: 10.1002/slct.201701204

CITATIONS

2

READS

280

5 authors, including:



Satinder K. Sharma

Indian Institute of Technology Mandi

110 PUBLICATIONS 610 CITATIONS

[SEE PROFILE](#)



Pawan Kumar

Okinawa Institute of Science and Technology

38 PUBLICATIONS 191 CITATIONS

[SEE PROFILE](#)



Sumit Barthwal

Kookmin University

16 PUBLICATIONS 213 CITATIONS

[SEE PROFILE](#)



Seema Sharma

Indian Institute of Technology Kanpur

40 PUBLICATIONS 594 CITATIONS

[SEE PROFILE](#)

Some of the authors of this publication are also working on these related projects:



Synthesis of carbon nano fibers, sieves [View project](#)

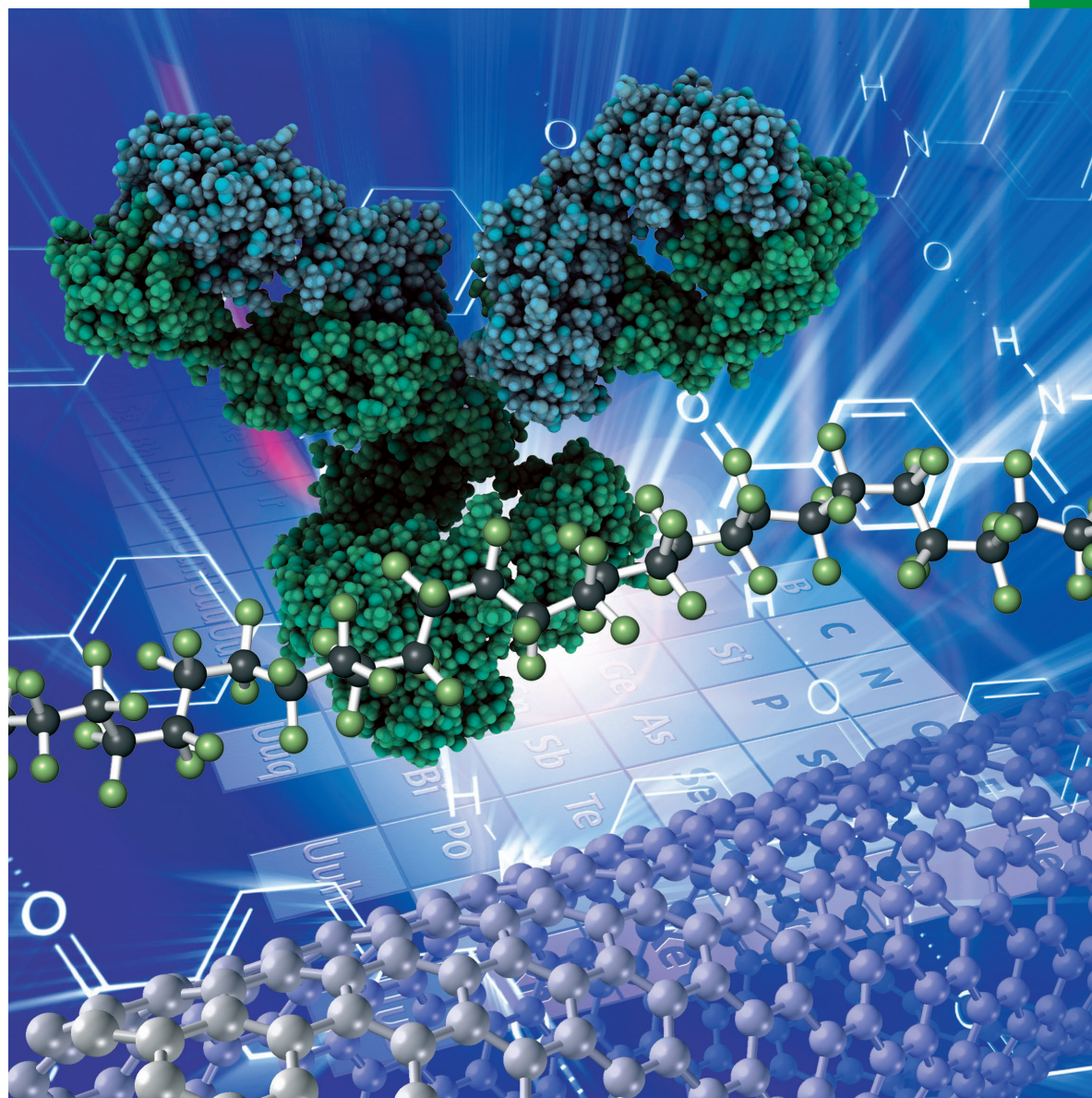


Electrospinning and Photocatalysis [View project](#)

Chemistry **SELECT** ✓

www.chemistryselect.org

A journal of



REPRINT

WILEY-VCH

Materials Science inc. Nanomaterials and Polymers

Highly Sensitive Surface-Enhanced Raman Scattering (SERS)- Based Multi Gas Sensor : Au Nanoparticles Decorated on Partially Embedded 2D Colloidal Crystals into Elastomer

Satinder K. Sharma,^{*[a, b]} Pawan Kumar,^[b] Sumit Barthwal,^[a] Seema Sharma,^[a] and Ashutosh Sharma^{*[a]}

Advent of surface-enhanced Raman spectroscopy (SERS) has engendered, the attention to exploit a facile, cost effective, 2D self-assembly based architecture for sensing. Here, Au nanoparticles are decorated on controlled morphology of 2D polystyrene colloidal crystals (PSCCs), partially embedded into flexible polydimethylsiloxane elastomer. Self-assembled flexible hexagonally close-packed PSCCs form the 75 and 25 nm voids in the 500 and 200 nm, PSCCs monolayers and act as an effective plasmonic propagator for SERS sensors signal. Optical and sensing response investigates with UV-Vis and Raman spectroscopy after the exposure of Au NP/2D PS CC/PDMS to

NH₃, H₂O₂, N₂O and H₂S gases environment. The increase in the SERS intensity at 491 cm⁻¹ for the 200 nm, CCs based sensors as compared to 500 nm, indicates that the sensing response, strongly dependent on the CCs size. The red-shift in the UV-Vis spectra and enhancement in intensity of SERS designate that H₂S forms the maximum Au NPs aggregates over the all tested gases. The chemisorptions on the phenyl ring, due to B₂ symmetric modes of the PSCCs with orthogonal polarizability of Au NPs, act as a hot spot for higher sensing response for the detection of gaseous precursors with higher SERS sensitivity and reliability.

Introduction

Recently, surface-enhanced Raman spectroscopy (SERS) has emerged as a promising technique for the highly surface-sensitive detection of chemical, biological, and environmental pollutants, with the technique capable of detecting single molecules.^[1] In addition, the SERS signal from excited surface plasmons is capable of detecting chemical and biological species at parts per million (ppm) levels, with the characteristics of the species as ascertained from the Raman signals. Therefore, it is a tremendously beneficial technique for many areas, like molecular electronics, chemical analysis, sensors for atmospheric monitoring (climate and pollution studies), in conjunction with the detection of harmful chemicals e.g., explosives and biological warfare agents,^[2,3] and medical diagnostics (glucose, DNA, etc.).^[2-14] Typically, the SERS effect occurs when a group of chemical/biological species is adsorbed onto plasmonic, nanostructured surfaces, such as Au, Ag, or Cu.^[15] The Raman signal

is enhanced by many orders of magnitude by the surface plasmons of the nanoparticles (NPs), especially when the plasmon frequency is in resonance with that of the probe radiation. This substantial amplification of the SERS signal is principally generated by two fundamental mechanisms: first, the electromagnetic field enhancement (EFE) that occurs through the localized fields of the nanostructures, and second, the chemical/electronic enhancement due to the increased Raman scattering cross-section when some lattices or chemical/biological species are adsorbed onto the surfaces of the nanostructures.^[16] Moreover, the EFE increases the SERS signal greatly when two or more NPs approach each other and form a 'hot spot',^[17] where the SERS signal may be locally enhanced by the excitation of local surface plasmons in the NPs.^[18] To achieve an effective SERS, the analytes must be adsorbed onto or near suitable nanostructures that can support surface plasmon excitations. Therefore, surface plasmon resonance (SPR) and SERS-based gas sensors have attracted much interest because of their potential for detecting various gaseous species.^[19] Myoung *et al.*^[20] have reported the fabrication of an SERS-based gas sensor composed of modified Ag NPs. Likewise, Wang *et al.*^[21] have demonstrated the SPR-based detection of O₂ with Au NPs embedded in SiO_x nanowires (NWs) under visible illumination at room temperature. Similarly, Tabassum *et al.*^[22] reported the SPR-based detection of H₂S gas by utilizing optical fibers coated with Cu-ZnO thin films. In addition, Mishra *et al.*^[23] and Jun *et al.*^[24] have developed an H₂ sensor by utilizing indium-tin oxide (ITO) thin films and high-sensitivity sensors with nano-cavity antenna arrays, respectively. Moreover,

[a] Dr. S. K. Sharma, Dr. S. Barthwal, Dr. S. Sharma, Prof. A. Sharma
Department of Chemical Engineering (CHE) & DST Unit on Nano Sciences
Indian Institute of Technology (IIT)-Kanpur
Kanpur, Uttar Pradesh 208016, India
E-mail: ashutos@iitk.ac.in

[b] Dr. S. K. Sharma, Dr. P. Kumar
School of Computing and Electrical Engineering
Indian Institute of Technology (IIT)-Mandi
Mandi, Himachal Pradesh 175001, India
E-mail: satinder@iitmandi.ac.in

Supporting information for this article is available on the WWW under <https://doi.org/10.1002/slct.201701204>

Rae *et al.*^[9] have demonstrated CO and N₂O sensors composed of mixed Ag/Pd NPs, while Biggs *et al.*^[25] have developed a chemical warfare agent (CWA) detector.

The gas sensing response of SERS-based sensors is rapid and more reliable than that of conventional sensors, although the understanding of such sensors is still in the nascent stages. The recent advancement of technology and nanostructure synthesis methods have made it possible to achieve sensing elements with various morphologies, such as NPs, holes, rods, pillars, slits, and disks.^[26–33] This diversity in the shape and size of nanostructures is accomplished via the implementation of cutting-edge techniques, including focused ion beam (FIB),^[34] electron beam lithography (EBL),^[35] nano-sphere lithography (NSL),^[36] and ion irradiation.^[37] However, these processes are generally slow, expensive, complex in procedures, and require sophisticated equipment or precise experimental controls. Therefore, to keep pace with the state-of-the-art sensor technology, there is a growing need to find suitable alternatives to reproduce cost-effective sensors with high throughput and large-area integration on flexible systems. Therefore, of all the chemical methods, the microemulsion synthetic route is the most promising compared to the other NP/nanostructure synthesis techniques, such as co-precipitation in solution, sol-gel, flame-spray pyrolysis, laser evaporation, and high-energy milling. This is because of the high versatility and reproducibility of microemulsion synthetic routes, as well as the simple equipment requirement, homogeneous mixing, controllable but narrow particle-size distributions, and noteworthy compositional control. Of the various sensing NPs available, Au NPs have received the most attention from the scientific community, especially for sensor applications, because of their chemical inertness, biological compatibility, and molecular labeling, where the singularities of SERS can be exploited to detect precursors.^[38] Thus, one of the most promising solutions is the fabrication of colloidal crystal (CC) templates partially embedded in the elastomer polydimethylsiloxane (PDMS) and then depositing SPR-active, size-tunable NPs on their surface to create flexible sensors. This approach offers the reproducibility of using close-packed, surface-confined arrays of flexible CCs partially embedded in the flexible PDMS elastomer. Such systems may be used as active flexible sensors for biological, chemisorption, and gaseous sensing applications.

Therefore, the lack of significant research in the field of flexible CC- and SERS-based sensor technology has paved the way for the simple synthesis of cost-effective, controlled morphology, microemulsion-based Au NPs for SERS applications. With a robust synthesis method, it is possible to integrate such Au NPs with flexible surfaces. In this study, self-assembled CC arrays with microemulsion-synthesized Au NPs attached to their surfaces and partially embedded in flexible PDMS substrates were investigated as a potential candidate for flexible gas sensing applications.

Results and Discussion

The 2D PSCCs gas sensors are characterized with FE-SEM, UV-Vis and Raman spectroscopies. Figure 1 shows FE-SEM images

of the highly ordered, hexagonal close-packed, 2D PSCCs partially embedded in the flexible PDMS substrate at different resolutions. Figure 1a and 1b show the FE-SEM images of the 500 nm diameter 2D PSCCs partially embedded in the PDMS surface at different magnifications (14.00 KX and 50.00 KX magnification, respectively), while Figure 1c and 1d show that of the 200-nm-diameter 2D PSCCs (25.00 KX and 50.00 KX magnification, respectively).

It can be seen from the FE-SEM images that the 2D PSCCs are uniformly distributed on the flexible PDMS substrates. The SPR-active Au NPs synthesized with the microemulsion (μ -emulsion) technique have an average particle size of 8 nm, as shown in Figure 2. Moreover, as depicts in the HR-TEM image, the μ -emulsion-based Au NPs are spherical in shape and uniformly distributed.

Figure 3 shows the FE-SEM images of the μ -emulsion based synthesized Au NPs deposited on the 2D PSCCs partially embedded in the flexible PDMS substrate. The shadows in Figure 3a and 3b confirm that the SERS-active Au NPs are deposited on the surface and in the voids of the partially embedded, highly organized, 500 and 200 nm diameter 2D PSCCs on the PDMS substrate. The voids in the 500 and 200 nm diameter 2D PSCCs are 75 and 25 nm, respectively, which are confirmed with the scale bar in the FE-SEM images. Indeed, the explicit packing distribution of the Au NPs onto the PSCCs is still a challenge chore to inspect through the AFM analysis, because in this measurement, AFM cantilever tip interact with soft PSCCs, which deform the PSCCs up to certain level and result in the blurry image of Au NPs on the PS colloidal crystal surface. Although, in the present study a reasonable, lower spring constant AFM cantilever is employed for the analysis. Besides this, from FE-SEM analysis with an increase in beam energy also mangle the PSCCs and result in the dull images. Withal, hither imaging analysis considered all these concerns.

For gas sensing applications, the adsorption of NH₃, N₂O, H₂ O₂, and H₂S gases by the Au NP/2D PSCC/PDMS sensor systems is characterized by UV-Vis spectroscopy. Figure 4 shows the UV-Vis spectra of the Au NP/2D PSCC/PDMS sensors exposed to NH₃, N₂O, H₂O₂, and H₂S gases. The UV-Vis spectra show the plasmon absorption bands of the Au NPs centered on 474 and 533 nm. The absorption bands in the short-wavelength/high-energy region (474 and 533 nm) are the typical peaks of Au NPs, with only minimal peak distortion present because of the uniform shape and size of the NPs.^[39] However, the absorption bands in the longer wavelength region, corresponding to 686 and 729 nm, might be due to the aggregation of Au NPs.

The possibility of aggregated Au NPs should not be ignored because after a sensor is exposed to a gas, the probability of Au NP aggregation is enhanced, as evidenced by the UV-Vis spectra in Figure 4. Therefore, the lower energy absorption bands represent the surface plasmon response of the Au NPs to the gases deposited on the surface of the partially embedded 2D PSCCs, and also because of the voids, on the surface of the elastomer matrix. In the literature, the UV-Vis absorption spectrum of 8 nm Au NPs on the surface of PSCCs has a maximum peak at $\lambda_{max} \approx 515$ nm.^[40] As shown in Figure 4, the maximum peaks in the absorption spectra are present at

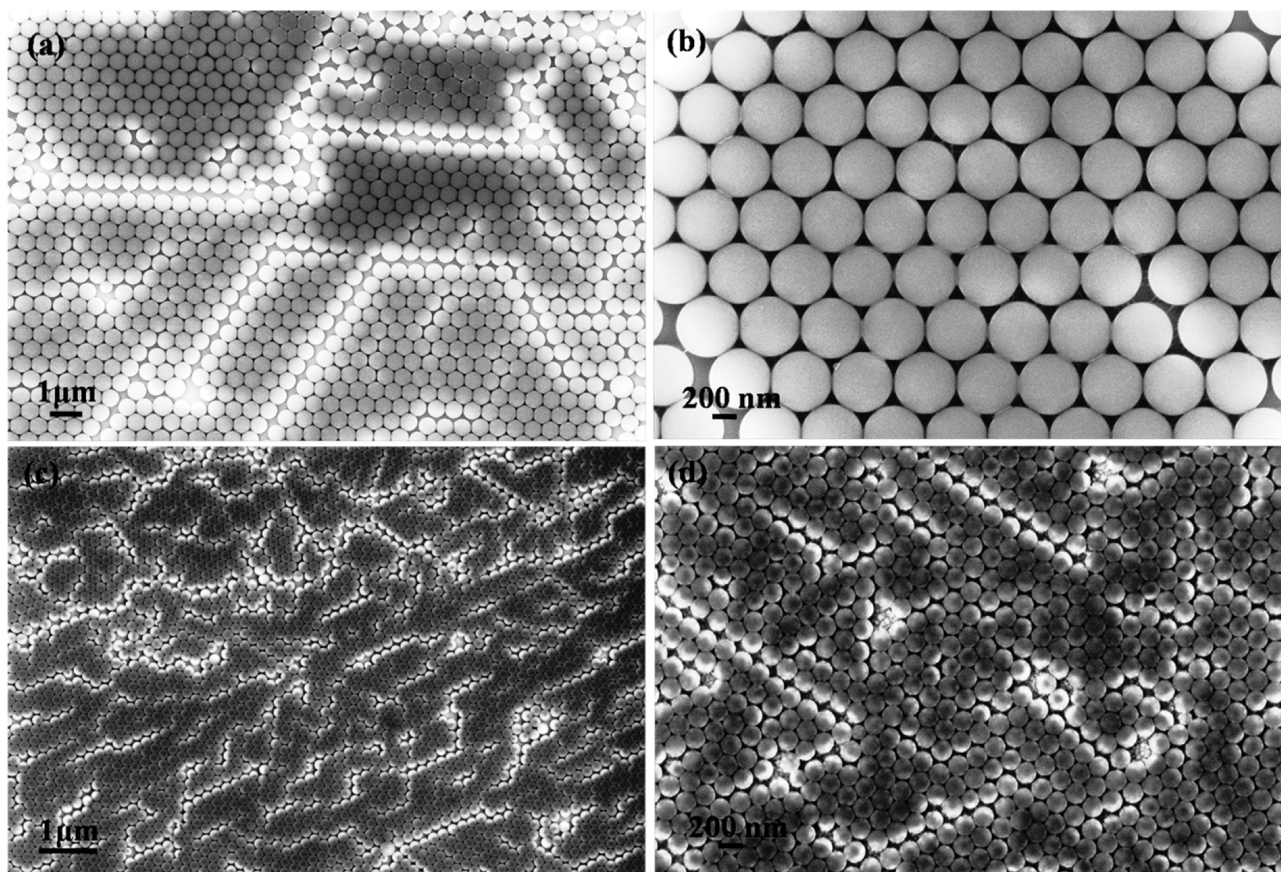


Figure 1. FE-SEM images of the highly ordered, hexagonal close-packed, ((a) and (b)) 500- and ((c) and (d)) 200-nm-diameter PSCCs partially embedded in the flexible PDMS substrate.

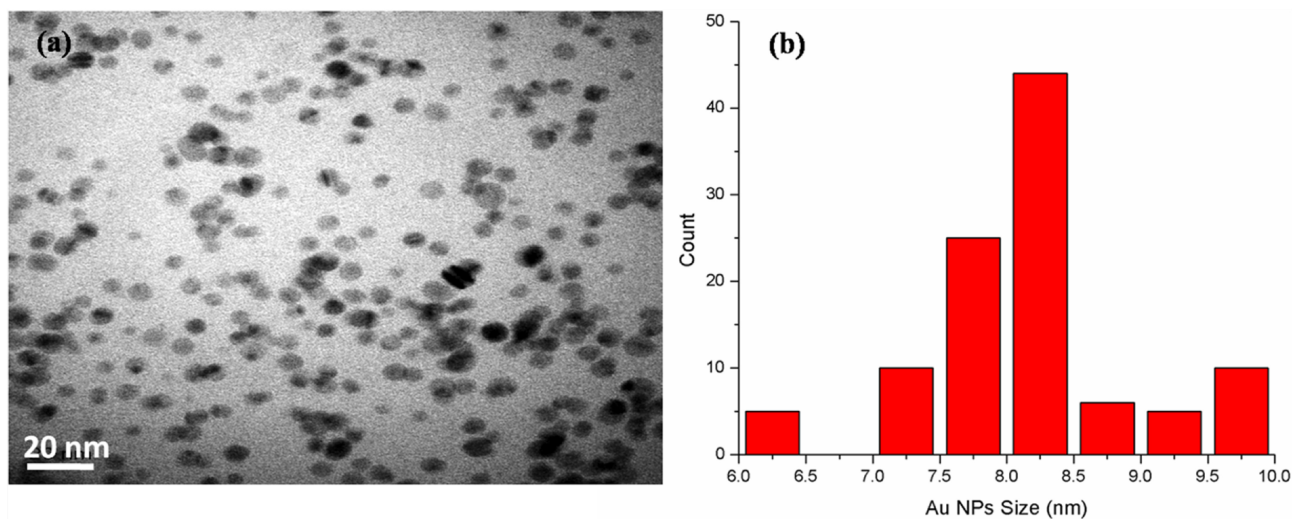


Figure 2. (a) HR-TEM image and (b) particle-size distribution of the Au NPs synthesized with the μ -emulsion route.

λ_{max} = 529, 533, 530, and 531 nm when the sensor is exposed to H_2O_2 , H_2S , N_2O , and NH_3 , respectively. Therefore, in present study, the interaction of the Au NPs with the NH_3 , N_2O , H_2O_2 ,

and H_2S gases causes a significant shift in the λ_{max} position (16, 15, 14, and 18 nm, respectively).

The largest redshift in the UV-Vis spectra is for the sensor highest number of Au NP aggregates to form as compared to

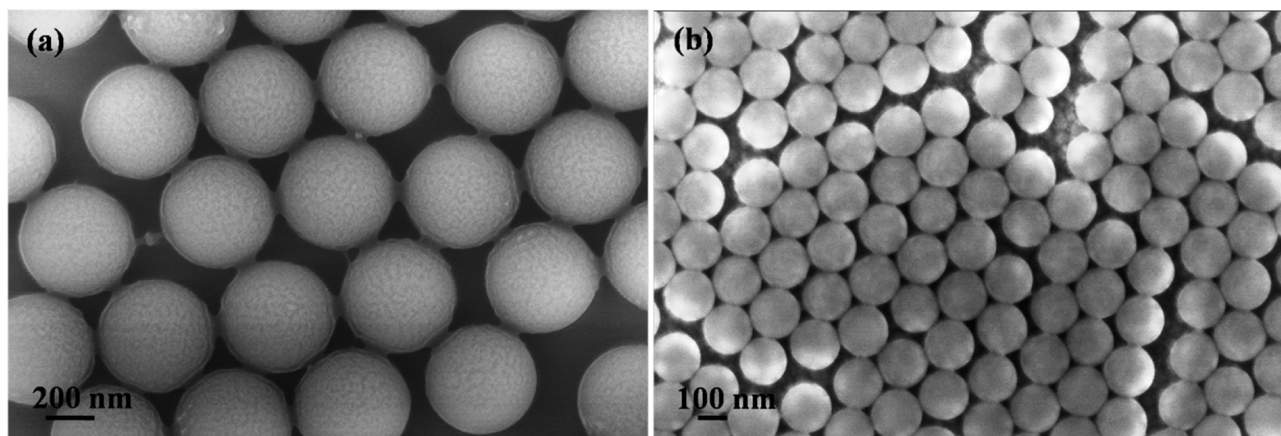


Figure 3. FE-SEM images of the (a) 500-nm and (b) 200-nm-diameter PSCCs coated with Au NPs.

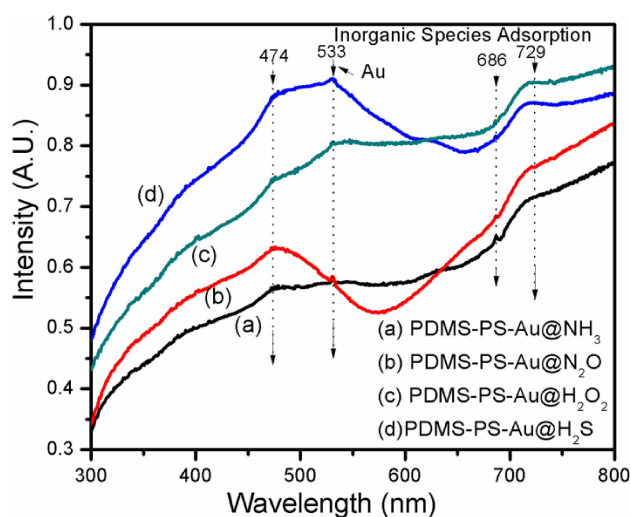


Figure 4. UV-Vis spectra of the (a) PDMS-PS-Au@NH₃, (b) PDMS-PS-Au@N₂O, (c) PDMS-PS-Au@H₂O₂, and (d) PDMS-PS-Au@H₂S systems.

the other gases tested. The two additional low-intensity peaks around 686 and 731 nm (Figure 4) are assigned to the adsorption of gas molecules onto the surface of the Au NPs, followed by the aggregation of these NPs. As shown in Figure 4, the maxima of the long-wavelength absorption peaks are at 718, 720, 727, and 729 nm for the NH₃, N₂O, H₂O₂, and H₂S gases, respectively. This indicates that the maximum SERS and absorption occurs when H₂S and H₂O₂ are adsorbed. This increase in intensity may not only depend on the adsorption of gases onto the surface of the Au NPs, but also due to imperfections on the surfaces of the NPs, lattice defects, etc. However, the aggregation of the Au NPs after the adsorption of gaseous species is the major factor.^[41–43] This aggregation results in strong coupling because of the dipole-dipole interactions that occur when the distance between adjacent NPs is typically smaller than the size of the NPs, which broadens the spectrum and also red shifts the plasmon band. Therefore, the significant red shift in the UV-Vis spectra might be the

result of smaller Au NPs agglomerating. This is a well-known phenomenon, where, because of the agglomeration of nanostructures, the shape of the UV-Vis spectra becomes broader and the plasmon band becomes asymmetrical after the exposure of sensors to the gaseous environment.^[41–43]

Therefore, taking into account these features; maximum red shift, increased intensity and considerable spectral broadening of the H₂S spectrum, indicates that the S–H and S–S bonds of H₂S are broken during the adsorption onto the surface of the Au NPs. The resulting molecular fragments are stabilized on the isolated Au NPs and are also more stable than the other gases tested.

The electromagnetic enhancement in SERS is the result of surface plasmon perturbations that are caused by the excitation-laser-induced polarization on the surface of the Au NPs. When the surface plasmons frequency and excitation source are in resonance, SERS is synergistically enhanced by the surface plasmons of the hexagonal close-packed arrays of Au NPs in the sensor system and the local fields of the Au NPs that are in the voids of the hexagonal close-packed 2D PSCCs partially embedded in the flexible elastomer substrate. The presence of Au NPs in the voids enhances the SERS intensity beyond just the polarization fields of the Au NP/2D PSCC/PDMS sensor system. It is thought that the enhanced local field of the 2D PSCC voids is proportional to the square of the applied field, especially under resonance conditions. When the deposited Au NPs (5–10 nm in diameter) are much smaller than the excitation wavelength (514.5 nm), the effective electric field (E_c) at resonance, according to the Rayleigh approximation, is given by Equation (1):^[44]

$$E_c = \frac{1}{1 + \left[\left(\frac{\epsilon(\omega)}{\epsilon_0} \right) - 1 \right] A} E_{inc} \quad (1)$$

Where A and E_{inc} are the depolarization factor and incident field on the particle, respectively, and $\epsilon(\omega)$ and ϵ_0 are the dielectric constants of the bulk and surrounding medium, respectively. It has been proven that coinage metals (Ag, Au,

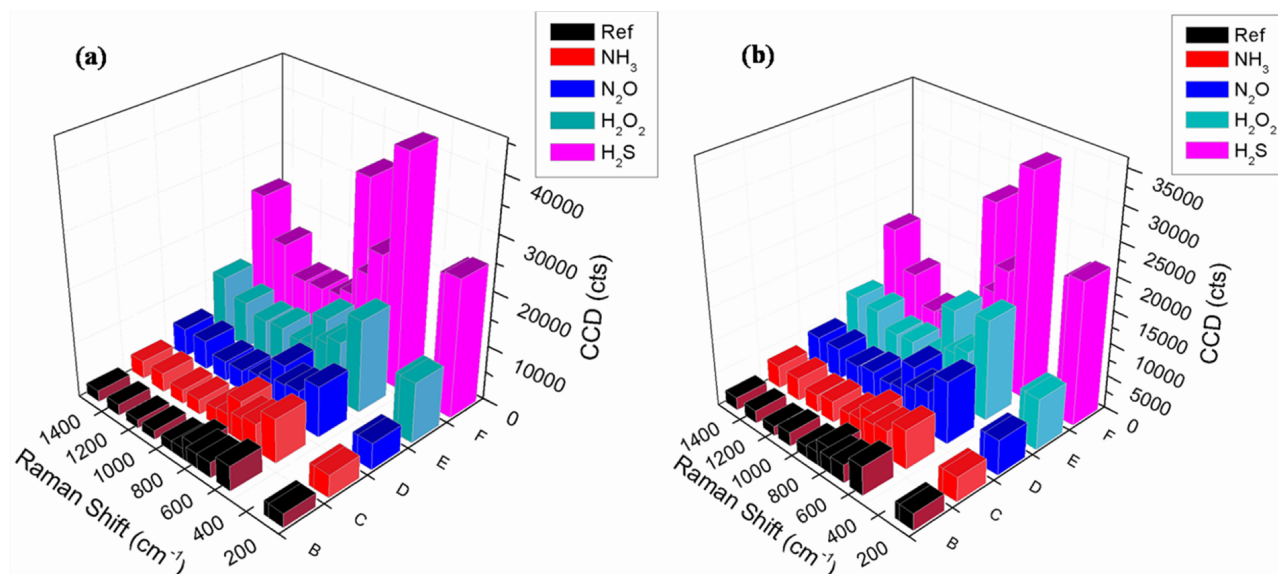


Figure 5. (a) SERS intensity variation for the flexible sensor with 200-nm-diameter PSCCs before and after exposure to various gaseous environments. (b) SERS intensity variation for the flexible sensor with 500 nm-diameter PSCCs before and after exposure to various gaseous environments.

Cu, etc.) have great potential for SERS-based applications because of the occurrence of enhanced E_c values in the visible region. Furthermore, Au NPs are more photo catalytically inert compared to the other metal NPs (Ag, Cu, etc.).^[45] This higher photoactivity of coinage-metal-based NPs, except for Au NPs, leads to the formation of derivative products during SERS analysis, which influences the characteristic SERS spectrum.^[41,44] Thus, in the present SERS study, the deposition of Au NPs on the 2D PSCC/PDMS flexible sensor system is investigated. The SERS excitation spectra for H_2O_2 , H_2S , N_2O , and NH_3 gases adsorbed onto the flexible Au NP/2D PSCC/PDMS systems are shown in Figure 5a and 5b. The values of E_c at the resonance of the gases adsorbed onto the flexible systems are much greater than the actually applied field. As stated in Equation (1), the resonance provides a considerable contribution from the local field of the Au NPs in the voids of the 2D PSCCs. In addition, the effective SERS effect of the flexible systems tested is also dependent upon other factors, such as the type of partially embedded 2D CCs, the size and density of the coinage metal NPs, and the excitation wavelength.^[40,45–47] As shown in the SERS spectra of the 200 nm diameter PSCC (Figure 5a) and 500 nm diameter PSCC (Figure 5b) devices, the characteristic peak intensities at 491 cm^{-1} are 6236, 7176, 12599, 36303 charge-coupled device counts (CCD cts) [200 nm] and 3729, 6985, 9116, and 29113 CCD cts [500 nm] for the NH_3 , N_2O , H_2O_2 , and H_2S gases, respectively. The significant enhancement in the SERS intensity at 491 cm^{-1} for the system with the 200 nm PSCCs compared to that with the 500 nm PSCCs is attributed to the size-dependent SERS effect of the 2D CCs when H_2O_2 , H_2S , N_2O and NH_3 gases are adsorbed onto the Au NPs/2D PSCC/PDMS flexible sensor system. In addition to this, the SERS enhancement of the proposed sensing system is a function of radiation damping, which becomes more severe as the size of

the 2D CCs increases because of the radiative losses of the electric dipole.^[41,44] The effective electrical strength (E_c) decreases with $1/r^3$, where r is the distance from the surface of the Au NPs.^[41,44]

Therefore, for SERS sensing, the active gaseous molecules need not be in direct contact with the surface of the SERS-active Au NPs, but can be located anywhere within the vicinity of the polarizing local fields of the NPs and voids.^[44] The results of this study show that using 500 nm PSCCs compared to 200 nm PSCCs in the proposed sensing system reduces the SERS intensity when they are exposed to various gases under identical conditions.

As shown in Figure 5a and 5b, the characteristic peaks of the spectra at 491, 615, 689, 713, 790, 864, 1003, 1121, and 1263 cm^{-1} represent the PSCCs.^[45] In particular, the peaks located at 689 and 864 cm^{-1} , and 615, 1003, and 1263 cm^{-1} correspond to the B_2 and B_1 symmetric modes of the PSCCs, respectively. This indicates that the polarizability of the phenyl ring in the 2D PSCCs is preferably oriented perpendicular to the B_2 symmetry (out-of-plane modes) at the surface of the deposited Au NPs. For the PS chemisorptions of Au–N, Au–O, and Au–S, the SERS interactions show their prominent signatures at 490 to 500 cm^{-1} . It is well established that the SERS intensity of PS is enhanced after being exposed to various gaseous environments, such as NH_3 , N_2O , H_2O_2 , and H_2S . As shown in Figure 5a and 5b, the Au–N stretch interaction contributes to the enhanced SERS intensity at 491 cm^{-1} when the sensor is exposed to NH_3 .^[49] Similarly, the N–O symmetric stretch contributes to the enhanced SERS intensity at 1263 cm^{-1} when the sensor is exposed to N_2O , and the enhancement at 491 cm^{-1} is due to the Au–O stretch interaction because of the dissociation of N–O bonds.^[50] For H_2O_2 exposure, the stretching and bending modes of O–O and

Table 1. variations of the SERS intensity (at 491 cm⁻¹) of Au NPs/2D PSCC/PDMS sensor system for different gases precursor exposure.

PS CCs Size (nm)	Without gas exposure (CCD cts)	NH ₃ gas exposure (CCD cts)	N ₂ O gas exposure (CCD cts)	H ₂ O ₂ gas exposure (CCD cts)	H ₂ S gas exposure (CCD cts)
500	2933	3729	6985	9116	29113
200	3078	6236	7176	12599	36303

O–H contribute to the SERS enhancement at 864 and 713 cm⁻¹, respectively.^[51] Furthermore, after H₂S exposure, the characteristic SERS peaks at 713 and 1003 cm⁻¹ are enhanced by the S–H stretching mode.^[52] The significant enhancement of SERS intensity at 491 cm⁻¹ (Figure 5a) when the sensor is exposed to NH₃ or N₂O is because of the Au–N stretching mode. Similarly, the enhancement with H₂O₂ and H₂S exposure is due to the Au–O and Au–S stretching modes, respectively.

Thus, the baseline SERS intensity at 491 cm⁻¹ for the flexible sensor system containing the 500 nm 2D PSCCs is 2933 CCD cts, and it increases to 3729, 6985, 9116, and 29113 CCD cts when the sensor is exposed to NH₃, N₂O, H₂O₂, and H₂S, respectively (Table 1). Similarly, the baseline SERS intensity for the sensor system with the 200 nm 2D PSCCs is 3078 CCD cts, and it increases to 6236, 7176, 12599, and 36303 CCD cts when the sensor is exposed to NH₃, N₂O, H₂O₂, and H₂S, respectively (Table 1). Therefore, the sensor with the 200 nm 2D PSCCs produces larger shifts in the SERS intensity compared to the sensor with the 500 nm PSCCs. This significant enhancement in the intensity shows that face-on (as discussed earlier, B₁ symmetric modes) is the only orientation for which the maximum absorption is achievable, especially for the extremely large absorption of the H₂S exposed sensor. In addition, the peaks at 1121 and 9261 cm⁻¹ in Figure 5a and 5b may be the result of degradation products forming when the sensors are irradiated with the excitation laser. This is because the Au NPs possess some level of photocatalytic activity that can influence the characteristic SERS spectrum.^[45] On the other hand, it is well established that the photocatalytic activity of Au NPs is size-dependent (< 5 nm) and occurs in the presence of oxides, like TiO₂, SiO₂, Al₂O₃, MgO, etc.^[45] Thus, the proposed Au NP/2D PSCC/PDMS flexible sensing system is more robust and quite unreactive for two reasons: (1) the Au NPs used in this flexible sensing system are larger than 5 nm and (2) are deposited on oxide-free 2D PSCCs that are partially embedded in the flexible elastomer substrate. As a result, it would be safe to state that the bands at 1121 and 1263 cm⁻¹ in the spectra shown in Figure 5a and 5b are not due to the presence of catalytic degradation products. Likewise, the bands around 160 and 189 cm⁻¹ correspond to Au–S–C bending modes that point towards the sulfate-terminated 2D PSCCs used in the Au NP/2D PSCC/PDMS flexible sensing system.^[48]

The variation in the SERS peak intensity of the flexible sensors after being exposed to NH₃, N₂O, H₂O₂, and H₂S gases are shown in Figure 5. The variation in SERS intensity for the Au NP/2D PSCC/PDMS flexible sensing systems can be explained with the enhancement factor, *G*, which is given by Equation. (2) and (3).^[41]

$$G = [(1 + 2g)(1 + 2g_o)]^2 \quad (2)$$

$$g = \frac{(m^2 - 1)}{(m^2 + 2)} \text{ and } g_o = \frac{(m_o^2 - 1)}{(m_o^2 + 2)} \quad (3)$$

Here, *m*₀ and *m* are the refractive indices of the medium for the incident and scattered radiation with frequencies of ω₀ and ω, respectively. The dielectric constant, κ, is related to *m* via κ = *m*². Eq. (2) can be used to calculate the SERS enhancement factor depending upon the refractive index or dielectric constant of the medium,^[53] with the dielectric constant a function of the polarizability of the medium. The atomic polarizability of the gases exposed to the Au NP/2D PS CC/PDMS flexible sensors follows the order NH₃ < H₂O₂ < N₂O < H₂S.^[54–57] This indicates that the refractive index change must be the greatest for H₂S exposure and should produce the maximum SERS enhancement, which is shown in Figure 5a and 5b. However, there are some disparities in Figure 5a and 5b that do not support these conclusions, e.g., the SERS intensity for H₂O₂ is 5423 counts higher than that of N₂O. This may be due to the oxidation of the surface of the Au NPs, which changes the dielectric constant near the Au NPs surfaces of the Au NP/2D PSCC/PDMS flexible sensors, and hence, increases the SERS intensity after H₂O₂ exposure.^[58]

Whereas, the steady conformity of all SERS signals are established by measuring the SERS response for the similar gaseous environment at four different regions on the fabricated SERS sensors. There is only 2–3% variation in the SERS signal intensity, noticed. Which clearly, attributes that the SERS signal from the fabricated sensors are quite consistent and reliable.

In order to confirm the variation in the SERS signal of fabricated sensors with the bending or strain is also investigated here. There is no significant change (~1–2%) in the SERS signal is found up to bending of 90°. While, previously^[59] taro leaf based PDMS replica work, observed that there is a variation in the SERS intensity on corresponds to the bending, where SERS signal was from the fixed analyte molecule position, separated from the plasmonic field. Other than, here the analyte molecule is gas and its random walk nature on the Au NPs surface result in the stable SERS signal.

Figure 6 shows the variation in sensor signals as functions of the concentration of NH₃, N₂O, H₂O₂, and H₂S to investigate the sensitivity of the sensors. The sensor signal (SERS) enhancement factor (*EF*) is estimated with Equation (4).^[19,60]

$$EF = \frac{I_{SERS}}{I_{RS}} \frac{P_{RS} T_{RS}}{P_{SERS} T_{SERS}} \quad (4)$$

where *I*_{SERS} is the SERS intensity, *I*_{RS} is the Raman intensity, *P*_{RS} is the laser power used for the Raman measurement, *P*_{SERS} is the laser power used for the SERS measurement, *T*_{RS} is the data acquisition

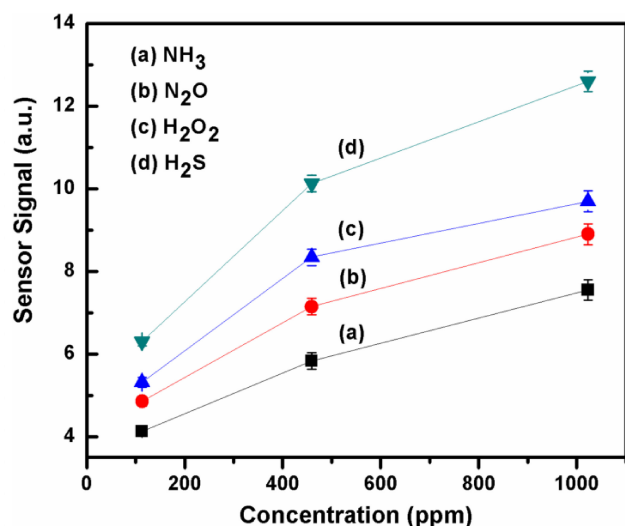


Figure 6. Plots showing the variation in sensor signals as functions of the concentration of the gases tested.

time of the Raman measurement, and T_{SERS} is the data acquisition time of the SERS measurement. The sensor signal variation indicates that the sensor signal increases with the concentration of the gases. The adsorption of analyte gas molecules onto the 2D PSCCs may also result in the agglomeration or densification of the Au NPs because of the deswelling of the 2D PSCCs in the Au NP/2D PSCC/PDMS flexible sensing systems.^[61] This process of deswelling and densification results in a considerable variation in the inter-particle distance of the Au NPs on the 2D PSCCs, concentrating more charges near the inter-particle junctions, which results in the formation of a "hot spot" and greatly enhances the SERS signal.^[60,43] It is thought that after the H₂S molecules are adsorbed onto the surface of the Au NPs, the full-scale agglomeration of Au NPs might occur compared to the other gases, which results in the maximum electromagnetic coupling between the discrete Au NPs and SERS signal. Similar behavior is exhibited by the sensors after the adsorption of H₂O₂ and is evidenced by the large signal compared to that after the adsorption of N₂O, which also supports the large-scale aggregation of Au NPs on the surfaces of the 2D PSCCs.

However, with respect to SERS enhancement, various attempts has been already reported in the literature, Yi *et al.* (2016)^[62] has studied SERS-based on Ag coating on self-assembled PSCC and Wang *et al.* (2014)^[63] demonstrated ~ 3 order improvement in detection limit of the SERS performance of Au film over PS nanospheres. Similarly, Chen *et al.* (2015) fabricate Au and Ag nanostructures over 3D ordered SiO₂ CC template and found increased SERS due to the presence of gaps in the rough nanostructure.^[64] Zhang *et al.* (2012) reported the SERS signal enhancement due to the coupling effect of periodically hexagonal packed Ag nanorods lattice and voids.^[65–67] Huang *et al.* (2016)^[68] demonstrated the SERS tuning through the lattice coupling based on variation in Au inter-rod gaps and heights. Whereas, in the present study used, Au NPs of 8 nm in dia, decorated on 2D PSCCs/PDMS system. The size dependent SERS phenomena has more susceptibility below 8 nm particle size, because at higher resolution NPs (<8 nm), the number of electric and magnetic multipole of the free

conduction electrons induced by an interacting electromagnetic field to amplify the collective oscillation will be more at plasmon resonance and consequence the significant shift with the reduction in particle size. Furthermore, the dielectric function of Au NPs is also a size dependent and rendering to a size-dependent absorption cross section due to intrinsic size effects. While for larger Au NPs (>8 nm) the cross section is also dependent on higher-order quadrupole, octopole based multipole modes and shift the plasmon resonance to longer wavelength and also broadening the band due to retardation effects.^[40] Thus, the magnitude of the SERS enhancement for uniform NPs (size and shape) can be describe in terms of the intrinsic damping that depends on the imaginary part of the dielectric constant of the Au NPs and the extrinsic damping that is proportional to the Au NPs polarizability, which increases with increase in size. The similar observations for self-assembled Au NPs are also reported elsewhere.^[39–40]

It clearly signifies that the self-assembled Au NPs decorated onto ordered 2D PSCC partially embedded in flexible PDMS elastomer and presence of Au NPs in nano voids formed due to self-assembly of 2D PSCCs/PDMS system have a coupling effect and significant contribution towards the SERS enhancement. The hexagonally periodic arranged Au NPs/2D PSCCs/PDMS system arc surface and the existence of NPs in the nano-voids act as a source of electromagnetic fields localization to the formulation of a promising "hot spot" to the SERS. Where the more adsorbed molecules probed and substantially increase the effective field of the array and result the enhancement in the responsivity and reproducibility of SERS signals.

The advantage of proposed and demonstrated Au NPs/2D PSCCs/PDMS system based SERS sensor substrate over the reported in the literature is that existing sensors mostly based on thin films provide less surface area for anylate adsorption as compare to the NPs. Besides this, another advantage is flexible PDMS substrate with the SERS dependence on the polarizability of the gas molecule and uniform/reproducible SERS signal compare to Ag colloid agglomeration over the Au PSCC, and nanostructured surface due to lack of control over shape and size.

There is limited literature^[9,69,70] available on the SERS based gas sensor, Biggs *et al.*^[69] reported a SERS sensor based on Ag film on nanosphere for the benzenethiol (BT) gas phase detection, with the detection limit 6 ppm at 356 K. Similarly, Rae *et al.*^[9] demonstrated SERS sensor for CO and N₂O using a mixed AgPd nanoparticle substrate to the detection limit up to the 10,000 ppm at 325 K. On the other hand, the SERS sensors fabricated and investigated in the present study have the detection limit less than 100 ppm at the room temperature (298 K). Thus, the SERS sensors demonstrated in the present studies have potential candidature for the gas sensor applications at room temperature. The various factors influence the SERS intensity of Au NP/2D PSCC/PDMS based flexible sensors, are the size of the PSCCs, hexagonal periodic closed packed ordered arrangement, self-assembly of Au NPs, presence of Au NPs in nano voids formed due to self-assembly of 2D PSCCs/PDMS system, the polarizability of the gaseous molecules and

Au NPs aggregation by the deswelling and densification of hexagonally closed packed PSCCs by gas molecule.

Furthermore, the recyclability/reusability issues of the developed multi gas SERS sensors need to address systematically, where the developed sensors can use in multiple times and its utility can be justified. Although, this study is not included here and will take account of in future communications, but there is a feasibility, where, recyclability apprehension of the investigated SERS sensors might be address, if the gaseous adsorbents are not kinetically and chemically prone to formation of everlasting chemical bonds with decorated Au NPs of Au NP/2D PSCC/PDMS flexible sensing systems.

Conclusions

This study has demonstrated the μ -emulsion-based controlled synthesis of Au NPs that are decorated onto the surface of 2D PSCCs partially embedded in a flexible PDMS elastomer substrate for gas sensing applications. The surface morphology of the PSCCs and sensing signals after being exposed to various gases NH_3 , H_2O_2 , N_2O , and H_2S are characterized with FE-SEM, UV-Vis and Raman spectroscopies. It was found that the 2D PSCCs are closely packed in a hexagonal arrangement and the variation in SERS intensity indicates the sensor signal dependency on the size of the 2D PSCCs, surface morphology, dimensions of the Au NPs, and size of the voids between the Au-NP-coated 2D PSCCs. The noticeable changes in the SERS intensity after the exposure to various gaseous environments, with the largest changes occurring after H_2S exposure, can be explained in terms of change in the local electric field, which is due to the agglomeration of Au NPs, and dielectric constant of the SERS-active medium. The SERS intensity exhibited a linear dependence on the polarizability of the gases tested, which is attributed to the coupling effects between the SPR of the Au NP islands and voids formed by the self-assembled 2D PSCCs arrays.

Acknowledgements

Dr. Satinder K. Sharma is grateful for the financial support from the Department of Science and Technology (DST), New Delhi, India, under a project of the Fast Track (Engineering Sciences) for Young Scientists scheme entitled "Surface Plasmon Based Flexible Colloidal Crystal Sensors, [SERC/ET-0003/2012]".

Conflict of Interest

The authors declare no conflict of interest.

Keywords: Au NPs • 2D colloidal crystal monolayer • Flexible elastomer • Microemulsion • Self-assembly • SERS sensors

- [1] X. Yu, J. Tao, Y. Shen, G. Liang, T. Liu, Y. Zhang, Q. J. Wang, *Nanoscale*, **2014**, *00*, 1.
- [2] O. M. Primera-Pedrozo, J. I. Jerez-Rozo, E. D. L. Cruz-Montoya, T. Luna-Pineda, L. C. Pacheco-Londoño, S. P. Hernández-Rivera, *IEEE Sensors J.* **2008**, *8*, 963.

- [3] P. R. Sajanlal, T. Pradeep, *Nanoscale* **2012**, *4*, 3427.
- [4] K. Ma, J. M. Yuen, N. C. Shah, J. T. Walsh Jr, M. R. Glucksberg, R. P. Van Duyn, *Anal. Chem.* **2011**, *83*, 9146.
- [5] C. R. Yonzon, D. A. Stuart, X. Zhang, A. D. McFarland, C. L. Haynes, R. P. Van Duyne, *Talanta* **2005**, *67*, 438.
- [6] M. Li, J. Zhang, S. Suri, L. J. Sooter, D. Ma, N. Wu, *Anal. Chem.* **2012**, *84*, 2837.
- [7] K. Chen, H. Han, Z. Luo, Y. Wang, X. Wang, *Biosens. Bioelectron.* **2012**, *34*, 118.
- [8] M. W. Sigrist, R. Bartlome, D. Marinov, J. M. Rey, D. E. Vogler, H. Wächter, *Appl. Phys. B* **2008**, *90*, 289.
- [9] S. I. Rae, I. Khan, *Analyst* **2010**, *135*, 1365.
- [10] P. G. Cao, R. N. Gu, Z. Q. Tian, *Langmuir* **2002**, *18*, 7609.
- [11] W. Chu, R. J. LeBlanc, C. T. Williams, J. Kubota, F. Zaera, *J. Phys. Chem. B* **2003**, *107*, 14365.
- [12] N. H. Kim, S. J. Lee, K. Kim, *Chem. Comm.* **2003**, *6*, 7245.
- [13] J. Ni, R. J. Lipert, G. B. Dawson, M. D. Porter, *Anal. Chem.* **1999**, *71*, 4903.
- [14] K. Kim, J.-Y. Choi, H. B. Lee, K. S. Shin, *J. Chem. Phys.* **2011**, *135*, 124705.
- [15] C. L. Haynes, C. R. Yonzon, X. Zhang, R. P. V. Duyne, *J. Raman Spectrosc.* **2005**, *36*, 471.
- [16] Y. Hu, J. Liao, D. Wang, G. Li, *Anal. Chem.* **2014**, *86*, 3955.
- [17] O. Péron, E. Rinnert, T. Toury, M. Lamy de la Chapelle, C. Compère, *Analyst* **2011**, *136*, 1018.
- [18] T. Q. N. Luong, T. A. Caoand, T. C. Dao, *Adv. Nat. Sci.: Nanosci. Nanotechnol.* **2013**, *4*, 015018.
- [19] K. H. Crowley, A. Morrín, R. L. Shepherd, M. in hetPanhuis, G. G. Wallace, M. R. Smyth, A. J. Killard, *IEEE Sensors J.* **2010**, *10*, 1419.
- [20] N. S. Myoung, H. K. Yoo, I. W. Hwang, *Synthesis and Photonics of Nanoscale Materials XI, Proc. SPIE* **2014**, 8969, 89690S.
- [21] S. B. Wang, Y. F. Huang, S. Chattopadhyay, S. J. Chang, R. S. Chen, C. W. Chong, M. S. Hu, L. C. Chen, K. H. Chen, *NPG Asia Mater.* **2013**, *5*, e49.
- [22] R. Tabassum, S. K. Mishra, B. D. Gupta, *Phys. Chem. Chem. Phys.* **2013**, *15*, 11868.
- [23] S. K. Mishra, B. D. Gupta, *Plasmonics* **2012**, *7*, 627.
- [24] Z. H. Jun, *Chin. Phys. B* **2012**, *21*, 087104.
- [25] K. B. Biggs, J. P. Camden, J. N. Anker, R. P. V. Duyne, *J. Phys. Chem. A* **2009**, *113*, 4581.
- [26] T. Chung, S. Y. Lee, E. Y. Song, H. Chun, B. Lee, *Sensors* **2011**, *11*, 10907.
- [27] S. Lincic, P. Christopher, D. B. Ingram, *Nat. Mater.* **2011**, *10*, 911.
- [28] L. M. Kukreja, S. Verma, D. A. Pathroseand, B. T. Rao, *J. Phys. D: Appl. Phys.* **2014**, *47*, 034015.
- [29] R. Jiang, B. Li, C. Fang, J. Wang, *Adv. Mater.* **2014**, *26*, 5274.
- [30] P. K. Jain, M. A. El-Sayed, *Chem. Phys. Lett.* **2010**, *487*, 153.
- [31] Z. Fan, X. Huang, C. Tan, H. Zhang, *Chem. Sci.* **2015**, *6*, 95.
- [32] R. G. Weiner, C. J. DeSantis, M. B. T. Cardoso, S. E. Skrabalak, *ACS Nano* **2014**, *8*, 8625.
- [33] N. Ortiz, S. E. Skrabalak, *Langmuir* **2014**, *30*, 6649.
- [34] Y.-Y. Lin, J.-D. Liao, Y. H. Ju, C.-W. Chang, A.-L. Shiau, *Nanotechnology* **2011**, *22*, 185308.
- [35] W. Yue, Z. Wang, Y. Yang, L. Chen, A. Syed, X. Wang, *J. Micromech. Microeng.* **2012**, *22*, 125007.
- [36] X. Ye, L. Qi, *Nano Today* **2011**, *6*, 608.
- [37] U. B. Singha, D. C. Agarwal, S. A. Khana, A. Tripathia, A. Kumar, R. K. Choudhury, B. K. Panigrahi, D. K. Avasthia, *Radiat. Eff. Defects Solids* **2011**, *166*, 553.
- [38] C. M. Niemeyer, *Angew. Chem. Int. Ed.* **2001**, *40*, 4128.
- [39] S. Hong, X. Li, *J. Nanomater.* **2013**, *2013*, 1.
- [40] J. Piella, N. G. Bastús, V. Puntès, *Chem. Mater.* **2016**, *28*, 1066–1075.
- [41] Q. Chen, Y. Rao, X. Ma, J. Dong, W. Qian, *Anal. Methods* **2011**, *3*, 274.
- [42] Y. Yokota, K. Ueno, H. Misawa, *Chem. Commun.* **2011**, *47*, 3505.
- [43] P. D. Robinson, A. Kassar, A. Sharma, T. Kukhtareva, C. W. Farley III, C. Smith, P. Ruffin, C. Brantley, E. Edwards, *J. Nanophotonics* **2013**, *7*, 073592.
- [44] T. Vo-Dinh, *Trends Anal. Chem.* **1998**, *17*, 557.
- [45] J. R. Anema, A. G. Brolo, A. Feltenb, C. Bittencourt, *J. Raman Spectrosc.* **2010**, *41*, 745.
- [46] R. A. Álvarez-Puebla, *J. Phys. Chem. Lett.* **2012**, *3*, 857.
- [47] N. Guillot, H. Shen, B. Frémaux, O. Péron, E. Rinnert, T. Toury, M. Lamy de la Chapelle, *Appl. Phys. Lett.* **2010**, *97*, 023113.
- [48] B. Varnholt, P. Oulevey, S. Luber, C. Kumara, A. Dass, T. Bürgi, *J. Phys. Chem. C* **2014**, *118*, 9604.

- [49] L. A. Sanchez, J. R. Lombardi, R. L. Birke, *Chem. Phys. Lett.* **1984**, *108*, 45.
- [50] S. Zou, R. Gómez, M. J. Weaver, *Langmuir* **1997**, *13*, 6713.
- [51] X. Li, A. A. Gewirth, *J. Raman Spectrosc.* **2005**, *36*, 715.
- [52] X. Li, D. Heryadi, A. A. Gewirth, *Langmuir* **2005**, *21*, 9251.
- [53] T. Wang, Z. Zhang, F. Liao, Q. Cai, Y. Li, S. T. Lee, M. Shao, *Sci. Rep.* **2014**, *4*, 4052.
- [54] S. J. A. Van Gisbergen, V. P. Osinga, O. V. Gritsenko, R. van Leeuwen, J. G. Sniijders, E. J. Baerends, *J. Chem. Phys.* **1996**, *105*, 3142.
- [55] P. K. Chattaraj, P. Fuentealba, P. Jaque, A. Toro-Labbé, *J. Phys. Chem. A* **1999**, *103*, 9307.
- [56] G. A. Maroulis, *J. Chem. Phys.* **1992**, *96*, 6048.
- [57] J. Koput, *Chem. Phys. Lett.* **1996**, *257*, 36.
- [58] G. Shan, S. Zheng, S. Chen, Y. Chen, Y. Liu, *Colloids Surf. B* **2013**, *102*, 327.
- [59] P. Kumar, R. Khosla, M. Soni, D. Deva, S. K. Sharma, *Sens. Actuators B* **2017**, *246*, 477.
- [60] J. H. Lee, M. A. Mahmoud, V. B. Sitterle, J. J. Sitterle, J. C. Meredith, *Chem. Mater.* **2009**, *21*, 5654.
- [61] K. B. Biggs, J. P. Camden, J. N. Anker, R. P. Van Duyne, *J. Phys. Chem. A* **2009**, *113*, 4581.
- [62] Z. Yi, G. Niu, J. Luo, X. Kang, W. Yao, W. Zhang, Y. Yi, Y. Yi, X. Ye, T. Duan, Y. Tang, *Sci. Rep.* **2016**, *6*, 32314.
- [63] J. F. Wang, X. Z. Wu, R. Xiao, P. T. Dong, C. G. Wang, *Plos One* **2014**, *9*, e97976.
- [64] J. Chen, G. Qin, W. Shen, Y. Li, B. Das, *J. Mater. Chem. C* **2015**, *3*, 1309.
- [65] S. L. Kleinman, R. R. Frontiera, A.-I. Henry, J. A. Dieringer, R. P. V. Duyne, *Phys. Chem. Chem. Phys.* **2013**, *15*, 21.
- [66] X. Zhang, Q. Zhou, W. Wang, L. Shen, Z. Li, Z. Zhang, *Mater. Res. Bull.* **2012**, *47*, 921–924.
- [67] X. Zhang, Q. Zhou, J. Ni, Z. Li, Z. Zhang, *Physica E* **2011**, *44*, 460–463.
- [68] Y. Huang, X. Zhang, E. Ringe, M. Hou, L. Ma, Z. Zhang, *Sci. Rep.* **2016**, *6*, 23159.
- [69] S. Yamazoe, M. Naya, M. Shiota, T. Morikawa, A. Kubo, T. Tani, T. Hishiki, T. Horiuchi, M. Suematsu, M. Kajimura, *ACS Nano* **2014**, *8*, 5622.
- [70] N. S. Myoung, H. K. Yoo, I. W. Hwang, *Synthesis and Photonics of Nanoscale Materials XI, Proc. of SPIE* **2010**, 8969, 89690S.

Submitted: May 31, 2017

Revised: August 6, 2017

Accepted: August 8, 2017